Quantum versus Classical Thermal Transport at Low Temperatures

Zhixing Zou,[1,2] Jiangbin Gong,[1,2,3] Jiao Wang,[4,5] Giulio Casati,[6,7] and Giuliano Benenti[6,8]
[1]Department of Physics, National University of Singapore, Singapore 117542, Singapore
[2]Centre for Quantum Technologies, National University of Singapore, Singapore 117543, Singapore
[3]MajuLab, CNRS-UCA-SU-NUS-NTU International Joint Research Unit, Singapore
[4]Department of Physics and Fujian Provincial Key Laboratory of Low Dimensional Condensed Matter Physics, Xiamen University, Xiamen 361005, Fujian, China
[5]Lanzhou Center for Theoretical Physics, Lanzhou University, Lanzhou 730000, Gansu, China
[6]Center for Nonlinear and Complex Systems, Dipartimento di Scienza e Alta Tecnologia, Università degli Studi dell'Insubria, via Valleggio 11, 22100 Como, Italy
[7]International Institute of Physics, Federal University of Rio Grande do Norte, Campus Universitário—Lagoa Nova, CP. 1613, Natal, Rio Grande Do Norte 59078-970, Brazil
[8]Istituto Nazionale di Fisica Nucleare, Sezione di Milano, via Celoria 16, 20133 Milano, Italy

(Received 29 September 2025; revised 15 December 2025; accepted 26 January 2026; published 11 February 2026)

This Letter aims to understand how quantum mechanics affects heat transport at low temperatures. In the classical setting, by considering a simple paradigmatic model, our simulations reveal the emergence of negative differential thermal resistance: paradoxically, increasing the temperature bias by lowering the cold bath temperature reduces the steady-state heat current. In sharp contrast, the quantum version of the model, treated via a Lindblad master equation, exhibits no negative differential thermal resistance: the heat current increases monotonically with thermal bias. This marked divergence highlights the fundamental role of quantum effects in low-temperature thermal transport and underscores the need to reconsider classical predictions when designing and optimizing nanoscale thermal devices.

DOI: 10.1103/zl25-tjt9

Introduction—Understanding the microscopic origins of macroscopic thermodynamic behavior is a central goal of statistical physics. Classical physics fails to reproduce certain thermodynamic quantities—most notably the heat capacity of materials at low temperatures [1–3]—a deficiency that was one of the key motivations for the development of quantum theory. A similar need to distinguish between classical and quantum predictions emerges in the context of nonequilibrium thermodynamics, particularly in the study of heat transport. This issue is driven both by fundamental scientific interest and by the rapid advancement of solid-state nanodevices, where thermal properties at low temperatures play a critical role [4]. Indeed, the ability to control and exploit the thermal transport properties of a system can result in devices such as thermal switches [5], thermal amplifiers [6], thermal logic gates [7], and thermal memories [8], which are at the core of a broad range of potential applications [4,9].

The implementation of the above-mentioned thermal devices relies on the realization of the thermal transistor [10–16], which in turn is grounded in the phenomenon of negative differential thermal resistance (NDTR) [7,10,17–29], recently observed in classical hard-core gas models [30,31]. Classical NDTR results so far have been obtained using the traditional Maxwell bath model [32], which assumes that particles thermalize instantaneously upon interaction with the bath. However, since the NDTR mechanism proposed in these studies involves cooling one of the baths to very low temperatures, the absence of a finite-rate relaxation process in the bath model may significantly affect the nonequilibrium steady state and, consequently, the resulting heat flux. Moreover, in the zero-temperature limit, a Maxwell bath instantaneously freezes colliding particles, which is an artificial feature in conflict with the third law of thermodynamics. These considerations give rise to the fundamental questions of whether NDTR is merely an artifact of the bath model or whether it reflects genuine features of classical dynamics. Furthermore, if the effect indeed originates from classical behavior, does it persist in a quantum mechanical framework? In other words, how does the heat current depend on the thermal gradient in the quantum regime at low temperatures?.

In this Letter, we investigate both classical and quantum heat transport in a paradigmatic nonlinear system: a single particle confined within a one-dimensional channel by a square-well potential, with the ends of the channel coupled

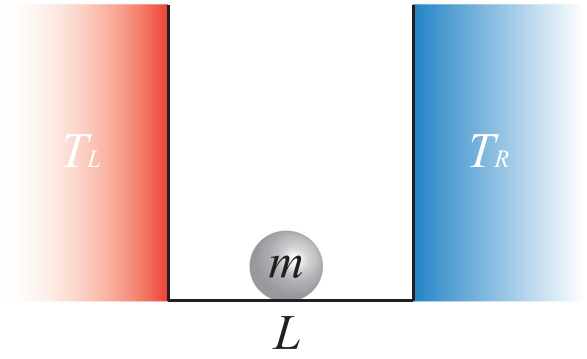

FIG. 1. Schematic plot of the one-dimensional infinite square-well system for heat transport. Each end of the system is connected to a thermal bath held at a different temperature.

to thermal reservoirs at different temperatures. This minimal model captures the fundamental features of heat transport at low temperatures and provides a direct basis for comparing classical and quantum behavior [33]. In the classical regime, we perform molecular dynamics simulations, and, to ensure consistency with the third law of thermodynamics, we incorporate relaxation dynamics into the bath model. Remarkably, even under these thermodynamically consistent conditions, NDTR still emerges, indicating that this phenomenon is an intrinsic feature of classical dynamics. This naturally raises the question of whether such a classical effect truly reflects physical reality, since low-temperature behavior is ultimately governed by quantum mechanics. We therefore extend our analysis to the quantum regime, modeling the system's dynamics using a Lindblad master equation carefully designed to reproduce classical thermal transport in the high-temperature limit. In stark contrast to the classical case, the quantum model exhibits no NDTR. These findings demonstrate that classical models can significantly mispredict thermal transport at low temperatures, highlighting the crucial role of quantum effects in this regime.

Classical modeling and results—As depicted in Fig. 1, we consider a particle of mass m confined within a one-dimensional channel of length L by a potential well. The system is described by the Hamiltonian

$$H = \frac{1}{2m}p^2 + V(x), \qquad V(x) = \begin{cases} 0, & 0 < x < L, \\ \infty, & \text{otherwise}, \end{cases} \tag{1}$$

with each end of the channel connected to a thermal bath at different temperatures. Because of the interaction between the particle and the two baths, the system evolves toward a nonequilibrium steady state in the long-time limit, characterized by a thermal flux.

In classical simulations, the bath is typically modeled as a Maxwell reservoir [32]: when the particle collides with bath $\alpha(\alpha = L, R)$, it is reflected with a random velocity v sampled from

$$f_\alpha(v) = \frac{m|v|}{k_B T_\alpha}\exp\left(-\frac{mv^2}{2k_B T_\alpha}\right), \tag{2}$$

where k_B is the Boltzmann constant.

According to the standard definition, the classical thermal flux J^c from the left bath to the right bath in our system is given by [see Supplemental Material (SM) [43] for the derivation]

$$J^c = \frac{E_{L\to R} - E_{R\to L}}{t_{L\to R} + t_{R\to L}}, \tag{3}$$

where $E_{L\to R}$ ($E_{R\to L}$) and $t_{L\to R}$ ($t_{R\to L}$) represent, respectively, the average energy the particle transfers and the average time it takes from the left (right) bath to the right (left) bath.

For a particle coupled to Maxwell baths, the thermal flux can be calculated analytically. The energy transferred from the left (right) bath during a single collision is $E_{L\to R,R\to L} = \int_0^\infty \frac{1}{2}mv^2 f_{L,R}(v)\mathrm{d}v = k_B T_{L,R}$ and the average time between successive collisions with the baths is $t_{L\to R,R\to L} = \int_0^\infty (L/|v|) f_{L,R}(v)\mathrm{d}v = L\sqrt{(m\pi/2k_B T_{L,R})}$. Substituting these expressions into Eq. (3), we obtain the classical thermal flux for the Maxwell bath,

$$J^c = \frac{k_B}{L}\sqrt{\frac{2k_B}{m\pi}}\sqrt{T_L T_R}(\sqrt{T_L} - \sqrt{T_R}). \tag{4}$$

The Maxwell bath approach assumes that the particle instantaneously reaches thermal equilibrium upon interacting with the bath. However, this assumption becomes problematic, particularly at low temperatures. Consider the extreme case of a bath at absolute zero ($T = 0$): under the Maxwell model, a collision with the bath would immediately reduce the particle's velocity to zero, effectively freezing it at the boundary. This behavior contradicts the third law of thermodynamics, which states that absolute zero cannot be reached in finite time. Consequently, the relaxation process cannot be neglected and must be properly accounted for.

To avoid such an unphysical scenario, we need to incorporate relaxation effects into the Maxwell bath. Relaxation is often described as a Markovian process, which can be conveniently modeled using the Markov chain Monte Carlo (MCMC) method [44]. In this approach, a Markovian transition matrix $\mathcal{T}(v \to v')$ with steady distribution $f_\alpha(v)$ is used. After a sufficiently large number of Monte Carlo steps, the Markov chain converges to this distribution, thereby generating the target ensemble. This naturally suggests interpreting the Markovian process in MCMC as a model that mimics the system's relaxation dynamics. We refer to this scheme as the "MCMC Maxwell bath model." This bath modeling mimics a temperature-dependent relaxation mechanism. In particular, we observe that the thermalization time diverges approximately as $T^{-0.9}$

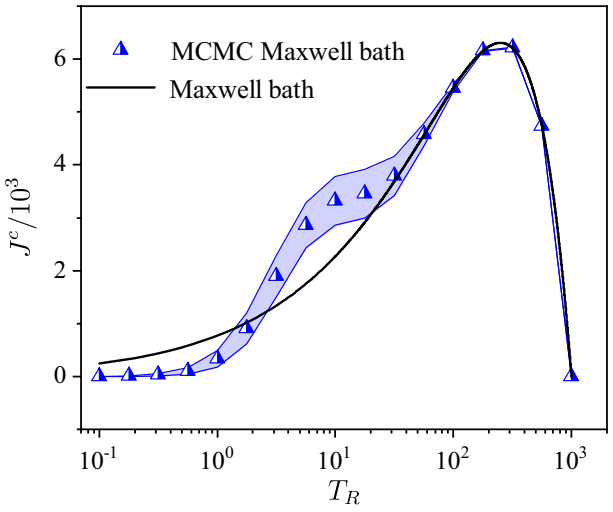

FIG. 2. Dependence of classical thermal flux with cold bath temperature T_R. The line is for result obtained with Maxwell baths [Eq. (4)], and the triangles are for MCMC Maxwell baths. The shaded region denotes the range of results obtained by varying the parameters of the MCMC Maxwell bath model (see SM [43] for details). In all simulations, we set $T_L = 10^3$, $m = 1$, $L = 1$, unless otherwise specified. Throughout this Letter we take $\hbar = 1$, $k_B = 1$, so that all physical quantities can be expressed in terms of a characteristic mass m_0 and a characteristic length L_0, both set equal to 1.

as the temperature T approaches absolute zero, which ensures consistency of the model with the third law of thermodynamics (see SM [43] for details).

In Fig. 2, the comparative results between traditional Maxwell baths and those implemented via MCMC are illustrated. When the cold bath temperature T_R is high, both models agree well, as the particle reflected by the MCMC Maxwell bath effectively relaxes to thermal equilibrium (see SM [43]). However, as T_R decreases, deviations emerge due to incomplete thermalization [45]. In the limit $T_R \to 0$, the thermal flux in both models approaches zero, but for fundamentally different reasons. In the traditional Maxwell bath, this behavior stems unphysically from a violation of the third law of thermodynamics: the particle instantaneously equilibrates with the cold bath, causing the time interval $t_{R\to L}$ in Eq. (3) to diverge. By contrast, in the MCMC Maxwell bath the vanishing flux results from the lack of relaxation at the cold bath, which causes the energy difference $E_{L\to R} - E_{R\to L}$ in Eq. (3) to approach 0. Clearly, both models exhibit the NDTR effect, as evidenced by the positive slopes of the J^c vs T_R plot in Fig. 2 over a wide range of T_R.

Quantum modeling and results—To simulate the quantum dynamics, we model the effect of the thermal baths using a Lindblad master equation [46], consistent with the Markovian framework adopted in the classical case above,

$$\frac{\mathrm{d}\hat{\rho}}{\mathrm{d}t} = -\frac{i}{\hbar}\left[\hat{H},\hat{\rho}\right] + \mathcal{D}_L(\hat{\rho}) + \mathcal{D}_R(\hat{\rho}) \equiv \mathcal{L}(\hat{\rho}), \tag{5}$$

where $\hat{\rho}$ is the density operator of the system, $\hbar$ is the Planck constant, and $\mathcal{D}_\alpha(\hat{\rho})$ is the dissipator term due to the interaction with bath α. The general expression of the dissipator term is given by [46]

$$\begin{aligned}\mathcal{D}_\alpha(\hat{\rho}) = \sum_{\omega>0} J(\omega)\Big\{&[1+n_\alpha(\omega)]\Big[\hat{A}_\alpha(\omega)\hat{\rho}\hat{A}_\alpha^\dagger(\omega) \\ &- 1/2\Big(\hat{A}_\alpha^\dagger(\omega)\hat{A}_\alpha(\omega)\hat{\rho} + \hat{\rho}\hat{A}_\alpha^\dagger(\omega)\hat{A}_\alpha(\omega)\Big)\Big] \\ &+ n_\alpha(\omega)\Big[\hat{A}_\alpha^\dagger(\omega)\hat{\rho}\hat{A}_\alpha(\omega) \\ &- 1/2\Big(\hat{A}_\alpha(\omega)\hat{A}_\alpha^\dagger(\omega)\hat{\rho} + \hat{\rho}\hat{A}_\alpha(\omega)\hat{A}_\alpha^\dagger(\omega)\Big)\Big]\Big\}. \end{aligned} \tag{6}$$

Here, $\hbar\omega = \epsilon_j - \epsilon_i$ is the energy difference of two eigenstates, $|\epsilon_j\rangle$ and $|\epsilon_i\rangle$ of H, $J(\omega)$ is the bath spectral function, $n_\alpha(\omega) = [\exp(\hbar\omega/k_B T_\alpha) - 1]^{-1}$ is the Bose-Einstein distribution characterizing the thermal state of bosonic baths, and the Lindblad operator $\hat{A}_\alpha(\omega)$ takes the form

$$\hat{A}_\alpha(\omega) = \sum_{i,j} |\epsilon_i\rangle\langle\epsilon_i|\hat{P}_\alpha|\epsilon_j\rangle\langle\epsilon_j|\delta_{\epsilon_j-\epsilon_i-\hbar\omega}, \tag{7}$$

which describes the transition induced by the bath through the system operator $\hat{P}_\alpha$. In our model, we write $\hat{P}_L$ and $\hat{P}_R$ as

$$\hat{P}_L \propto \int_0^\delta |x\rangle\langle x|\mathrm{d}x, \qquad \hat{P}_R \propto \int_{L-\delta}^{L} |x\rangle\langle x|\mathrm{d}x, \tag{8}$$

where δ is a small parameter representing the spatial range at the boundaries over which the system interacts with the baths. The δ-dependent prefactors of $\hat{P}_L$ and $\hat{P}_R$ in Eq. (8) are determined by requiring well-behaved matrix elements of operators $\hat{A}_\alpha(\omega)$ in the limit of $\delta \to 0$ [see SM [43] for the derivation and the explicit form of the operators $\hat{A}_\alpha(\omega)$].

The quantum thermal flux can be calculated using the continuity equation for energy,

$$\frac{\mathrm{d}}{\mathrm{d}t}\mathrm{Tr}[\hat{\rho}\,\hat{H}] = J_L - J_R, \tag{9}$$

where

$$J_L = \mathrm{Tr}[\mathcal{D}_L(\hat{\rho})\hat{H}] \quad \text{and} \quad J_R = -\mathrm{Tr}[\mathcal{D}_R(\hat{\rho})\hat{H}] \tag{10}$$

denote the thermal flux from the left and right bath to the system, respectively. In the steady state $\hat{\rho}_s$ the quantum thermal flux J^q from the left bath to the right baths is given by

$$J^q = J_L = -J_R. \tag{11}$$

In the quantum model, the steady state is calculated from the stationary solution of equation $\mathcal{L}(\hat{\rho}) = 0$ [40]. We solve the equation by finding the eigenvector of the superoperator

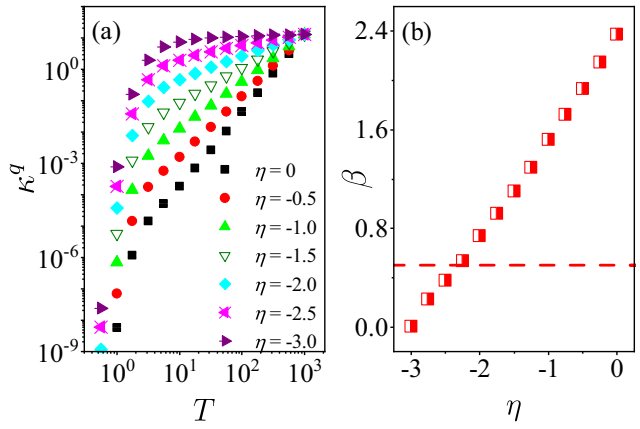

FIG. 3. (a) Temperature dependence of thermal conductivity for different bath spectral functions $J(\omega) = \gamma\omega_c^{1-\eta}\omega^\eta$, where γ is always set through the relation $\kappa^q(T_{\max}) = \kappa^c(T_{\max})$. For $\eta = 0$, -0.5, -1.0, -1.5, -2.0, -2.5, and -3.0, the corresponding values of γ are 8.036×10^{-7}, 3.755×10^{-5}, 1.477×10^{-3}, 4.691×10^{-2}, 1.160, 22.499, and 357.057, respectively. Note that for all values of ω corresponding to transitions between energy eigenstates, i.e., $\hbar\omega = \epsilon_j - \epsilon_i$, the condition that the relaxation time is much shorter than the timescale of the intrinsic evolution of the system [46], i.e. $\gamma J(\omega) \ll \omega$, is satisfied. (b) Relation between the exponent β and the exponent η. The dashed line is for $\beta = \beta_{\rm cl}$. Hereafter, we set $\omega_c = 1$.

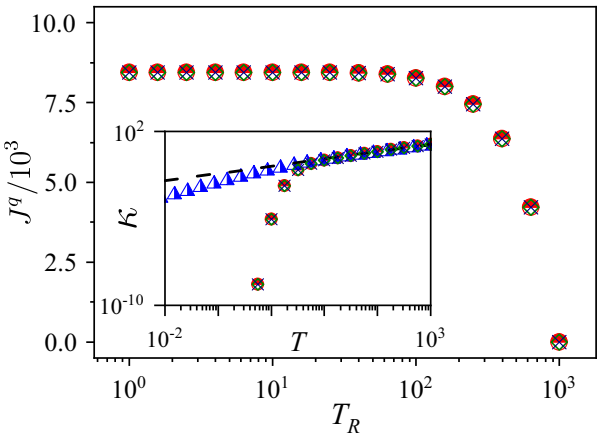

FIG. 4. Dependence of quantum thermal flux with cold bath temperature T_R, with $T_L = 10^3$. The inset shows the temperature dependence of κ. Olive squares, red circles, and navy crosses represent quantum results computed with Hilbert space cutoffs $N_{\rm tru} = 80$, 100, and 120, respectively, blue triangles are for classical results with MCMC Maxwell bath, and the dashed line is for the result of classical system with Maxwell baths [Eq. (12)].

$\mathcal{L}$ corresponding to the zero eigenvalue. Although the dimension of Hilbert space is infinite, it is reasonable to truncate it to $N_{\rm tru}$ energy levels, ensuring that the condition $\exp[-(\epsilon_{N_{\rm tru}} - \epsilon_1)/k_B T_{\max}] \ll 1$ holds ($T_{\max}$ is the maximum temperature in our simulations). We set $N_{\rm tru} = 100$ and $T_{\max} = 1000$ to guarantee that this condition is met.

Note that in the infinite square-well system, there is a finite minimum energy gap given by $\hbar\omega_{\min} = \epsilon_2 - \epsilon_1$. Since the spectral function $J(\omega)$ affects the dynamics only for frequencies $\omega > \omega_{\min}$, we are free to adopt the form $J(\omega) = \gamma\omega_c^{1-\eta}\omega^\eta$ within the actual frequency range $\omega > \omega_{\min}$, even for negative η. Indeed, we still always assume $J(\omega) \to 0$ as $\omega \to 0$ so that $J(\omega)$ remains a physical spectral function [46].

To proceed with our quantum model analysis, it is necessary to determine the strength γ and the exponent η in the spectral function $J(\omega)$. To achieve this, we ensure quantum-classical correspondence for the thermal conductivity κ in the high-temperature regime. Note that our definition of κ deviates from the standard one $\kappa_{\rm std}$ commonly used in systems with finite particle *density*: we divide the thermal flux by the temperature difference Δ rather than by the temperature gradient Δ/L, so that $\kappa = \kappa_{\rm std}/L$. We first match the thermal conductivity at the highest temperature, i.e., $\kappa^q(T_{\max}) = \kappa^c(T_{\max})$. Figure 3(a) shows the temperature dependence of the thermal conductivity for different spectral functions of the form $J(\omega) = \gamma\omega_c^{1-\eta}\omega^\eta$ for $\omega \geq \omega_{\min}$. In the high-temperature regime, the quantum thermal conductivity follows a scaling behavior $\kappa^q \propto T^\beta$, where β is an η-dependent exponent. Notably, this temperature-dependent scaling has a parallel in classical systems. For a classical system at high temperature that can be well modeled with Maxwell baths, consider the case where $T_L = T + (\Delta/2)$, $T_R = T - (\Delta/2)$. As the temperature difference Δ between the two baths approaches zero, Eq. (4) predicts that the classical thermal conductivity also follows a power-law scaling given by

$$\kappa^c = \lim_{\Delta\to 0} \frac{J^c}{\Delta} = \frac{k_B}{L}\sqrt{\frac{k_B T}{2m\pi}} \propto T^{1/2}. \tag{12}$$

To fully determine the bath spectral function $J(\omega)$, we impose an additional restriction: the quantum system must reproduce the same temperature-dependent behavior of the thermal conductivity as observed in the classical system in the high-temperature regime, i.e., $\beta = \beta_{\rm cl} = \frac{1}{2}$. From the relation between β and η [shown in Fig. 3(b)], we can extract an approximation for the value of η that satisfies this condition, yielding $\eta \approx -2.25$.

After determining the full bath spectral function, we analyze both the relaxation dynamics (see SM [43]) and thermal transport properties of the open square-well model. The dependence of the quantum thermal flux J^q on the cold bath temperature T_R is shown in Fig. 4. Notably no NDTR is observed: the plotted curve of J_q vs T_R has no positive slope over the entire range of T_R. To account for the absence of quantum NDTR observed here, we propose the following physical mechanism. In the classical case, thermodynamically consistent NDTR arises from the vanishing relaxation rate of the cold reservoir in the zero-temperature limit, which suppresses energy exchange with that reservoir and ultimately leads to a breakdown of heat transport.

In contrast, the wavelike nature of the quantum particle enables continuous interaction with both thermal reservoirs, even at very low temperatures. Consequently, the classical mechanism responsible for NDTR is no longer operative in the quantum regime, and hence NDTR does not emerge.

To further validate our approach, we present in the inset the temperature dependence of the thermal conductivity, defined within the linear response regime. At high temperatures, the quantum system indeed reproduces the same temperature scaling of thermal conductivity as its classical counterpart. In the low-temperature regime, both the quantum results and those from the MCMC Maxwell bath deviate from the scaling law (12), with the quantum case exhibiting a pronounced superexponential decay in thermal conductivity. This quantum deviation from the classical thermal transport behavior indicates that the discreteness of the energy spectrum hinders bath-induced energy transitions at temperatures below the smallest energy gap between eigenstates, i.e., when $k_B T \ll \epsilon_2 - \epsilon_1$.

Finally, we comment on the quantum-to-classical transition in our model. By applying the scaling $\gamma \to \gamma L^{-0.5}$, the quantum system exhibits a heat flux with the same L dependence as in the classical case (see simulation results in SM [43]). This correspondence can be understood through the following scaling analysis. To keep the Bose-Einstein distributions $n_\alpha[(\epsilon_j - \epsilon_i)/\hbar]$ in Eq. (5) invariant under changes in the system size L, the temperature must scale as T/L^2. With this scaling, the quantum heat flux becomes $J^q(T_L/L^2, T_R/L^2) \sim (\gamma L^{-0.5})(L^{-2})^{-2.25}(L^{-3})^2 L^{-2} \sim L^{-4}$, where the second term comes from the spectral density $J(\omega)$, the third from the Lindblad operators, and the last from the temperature difference between the baths. In the classical case, using Eq. (4), the heat flux under the same temperature scaling also follows $J^c(T_L/L^2, T_R/L^2) \sim L^{-4}$. Therefore, the quantum and classical heat fluxes share the same L dependence, provided γ scales as $L^{-0.5}$. A natural consequence of this scaling behavior is that increasing $T_{\max}$ at fixed L is equivalent to increasing L at fixed $T_{\max}$—that is, both operations drive the quantum system toward the classical limit.

Conclusions and discussion—In summary, we have investigated thermal transport in a paradigmatic nonlinear system. On the classical side, using MCMC Maxwell baths to incorporate temperature-dependent relaxation effects, we observed the NDTR effect. On the quantum side, we modeled the system using a Lindblad master equation to describe interactions with thermal baths. By appropriately designing the bath spectral function, the quantum model accurately reproduces the classical temperature dependence of thermal conductivity in the high-temperature regime. However, in stark contrast to the classical case, no evidence of NDTR is observed at low temperatures. These findings provide a foundational step toward understanding low-temperature thermal transport and may have practical implications for the design of nanoscale thermal devices. To confirm the generality of our results, we show in the End Matter that they remain qualitatively unchanged when considering two interacting hard-point colliding particles, a paradigmatic model in the study of classical heat transport [47–49], or when using the Redfield equation—which does not assume the rotating wave approximation—instead of the Lindblad equation. From a theoretical perspective, extending this analysis beyond phenomenological open-system models to fully microscopic descriptions—both classical and quantum–remains an important and challenging direction for future research. In particular, addressing the complexities introduced by strong coupling [50–52] and non-Markovian dynamics [53–59] will be essential for establishing a more comprehensive framework.

Beyond purely thermal transport, billiardlike gas models provide a versatile platform for exploring coupled transport phenomena, such as thermoelectric effects [34,35]. Extending the present framework to investigate coupled transport in both classical and quantum open systems represents a promising avenue for future research. Such studies could yield valuable insights for the design of nanoscale energy conversion technologies [60] and quantum thermoelectric devices.

Acknowledgments—J. G. acknowledges support by the National Research Foundation, Singapore through the National Quantum Office, hosted in A*STAR, under its Centre for Quantum Technologies Funding Initiative (No. S24Q2d0009). J. W. is supported by the Natural Science Foundation of China (Grant No. 12475038) and the National Key R&D Program of China (Grant No. 2023YFA1407100) and G. B. acknowledges support from INFN through the project QUANTUM. We thank the anonymous referees for comments that helped improve the manuscript.

Data availability—The data that support the findings of this article are not publicly available. The data are available from the authors upon reasonable request.

[1] A. Einstein, Ann. Phys. (Berlin) **22**, 180 (1907).
[2] P. Debye, Ann. Phys. (Berlin) **344**, 789 (1912).
[3] C. Kittel, *Introduction to Solid State Physics*, 8th ed. (Wiley, New York, 2005).
[4] J. P. Pekola and B. Karimi, Rev. Mod. Phys. **93**, 041001 (2021).
[5] G. Wehmeyer, T. Yabuki, C. Monachon, J. Wu, and C. Dames, Appl. Phys. Rev. **4**, 041304 (2017).
[6] W.-R. Zhong, D.-Q. Zheng, and B. Hu, Nanoscale **4**, 5217 (2012).
[7] L. Wang and B. Li, Phys. Rev. Lett. **99**, 177208 (2007).
[8] L. Wang and B. Li, Phys. Rev. Lett. **101**, 267203 (2008).
[9] N. Li, J. Ren, L. Wang, G. Zhang, P. Hänggi, and B. Li, Rev. Mod. Phys. **84**, 1045 (2012).
[10] B. Li, L. Wang, and G. Casati, Appl. Phys. Lett. **88**, 143501 (2006).

[11] K. Joulain, J. Drevillon, Y. Ezzahri, and J. Ordonez-Miranda, Phys. Rev. Lett. **116**, 200601 (2016).
[12] A. Sood, F. Xiong, S. Chen, H. Wang, D. Selli, J. Zhang, C. J. McClellan, J. Sun, D. Donadio, Y. Cui, E. Pop, and K. E. Goodson, Nat. Commun. **9**, 4510 (2018).
[13] J. Wang, G. Casati, and G. Benenti, Phys. Rev. Lett. **124**, 110607 (2020).
[14] Y. Li, Y. Dang, S. Zhang, X. Li, Y. Jin, P. Ben-Abdallah, J. Xu, and Y. Ma, Phys. Rev. Appl. **20**, 024061 (2023).
[15] L. Castelli, Q. Zhu, T. J. Shimokusu, and G. Wehmeyer, Nat. Commun. **14**, 393 (2023).
[16] J. W. Lim, A. Majumder, R. Mittapally, A.-R. Gutierrez, Y. Luan, E. Meyhofer, and P. Reddy, Nat. Commun. **15**, 5584 (2024).
[17] B. Li, L. Wang, and G. Casati, Phys. Rev. Lett. **93**, 184301 (2004).
[18] D. Segal, Phys. Rev. B **73**, 205415 (2006).
[19] N. Yang, N. Li, L. Wang, and B. Li, Phys. Rev. B **76**, 020301(R) (2007).
[20] W. Chung Lo, L. Wang, and B. Li, J. Phys. Soc. Jpn. **77**, 054402 (2008).
[21] W.-R. Zhong, P. Yang, B.-Q. Ai, Z.-G. Shao, and B. Hu, Phys. Rev. E **79**, 050103(R) (2009).
[22] Z.-G. Shao, L. Yang, H.-K. Chan, and B. Hu, Phys. Rev. E **79**, 061119 (2009).
[23] D. He, S. Buyukdagli, and B. Hu, Phys. Rev. B **80**, 104302 (2009).
[24] D. He, B.-Q. Ai, H.-K. Chan, and B. Hu, Phys. Rev. E **81**, 041131 (2010).
[25] E. Pereira, Phys. Rev. E **82**, 040101(R) (2010).
[26] W.-R. Zhong, M.-P. Zhang, B.-Q. Ai, and B. Hu, Phys. Rev. E **84**, 031130 (2011).
[27] W. Fu, T. Jin, D. He, and S. Qu, Physica (Amsterdam) **433A**, 211 (2015).
[28] H.-K. Chan, D. He, and B. Hu, Phys. Rev. E **89**, 052126 (2014).
[29] M. S. Mendonça and E. Pereira, Phys. Lett. A **379**, 1983 (2015).
[30] R. Luo, Phys. Rev. E **99**, 032138 (2019).
[31] R. Luo, J. Guo, J. Zhang, and H. Yang, Phys. Rev. Res. **4**, 043184 (2022).
[32] J. L. Lebowitz and H. Spohn, J. Stat. Phys. **19**, 633 (1978).
[33] This model represents the simplest instance of billiard-type gas models, which serve as paradigms in the study of classical nonequilibrium dynamics due to their conceptual simplicity and dynamical richness [13,30–32,34–39]. In contrast, studies of quantum thermal transport have predominantly focused on spin chain and tight-binding systems [40–42]. This preference likely stems from the intrinsic difficulty of modeling collisional interactions between gas particles and thermal baths in the quantum regime.
[34] G. Benenti, G. Casati, and J. Wang, Phys. Rev. Lett. **110**, 070604 (2013).
[35] R. Luo, G. Benenti, G. Casati, and J. Wang, Phys. Rev. Lett. **121**, 080602 (2018).
[36] C. P. Dettmann, The Lorentz gas: A paradigm for nonequilibrium stationary states, in *Hard Ball Systems and the Lorentz Gas*, edited by D. Szász (Springer, Berlin, Heidelberg, 2000), pp. 315–365.
[37] B. Li, G. Casati, J. Wang, and T. Prosen, Phys. Rev. Lett. **92**, 254301 (2004).
[38] J. Wang and G. Casati, Phys. Rev. Lett. **118**, 040601 (2017).
[39] Z. Zou, G. Casati, G. Benenti, and J. Wang, Phys. Rev. E **109**, L062104 (2024).
[40] G. T. Landi, D. Poletti, and G. Schaller, Rev. Mod. Phys. **94**, 045006 (2022).
[41] V. Balachandran, G. Benenti, E. Pereira, G. Casati, and D. Poletti, Phys. Rev. Lett. **120**, 200603 (2018).
[42] V. Balachandran, G. Benenti, E. Pereira, G. Casati, and D. Poletti, Phys. Rev. E **99**, 032136 (2019).
[43] See Supplemental Material at http://link.aps.org/supplemental/10.1103/zl25-tjt9 for the derivation of classical thermal flux [Eq. (3)], details of the MCMC Maxwell bath relaxation and robustness checks, explicit expressions of the dissipator terms and Lindblad operators, quantum relaxation analysis, the length-scaling comparison, and numerical details for the two-interacting-particles model.
[44] D. W. Heermann, Stochastic methods, in *Computer Simulation Methods in Theoretical Physics* (Springer, Berlin, Heidelberg, 1986), pp. 56–108.
[45] In the MCMC Maxwell bath, incomplete relaxation leads to an effective temperature T_{eff} of the particle reflected from the cold bath that is higher than the prescribed bath temperature T_R. When T_{eff} only slightly exceeds T_R, this enhancement results in a larger heat flux compared to the standard Maxwell bath, owing to the NDTR effect. At the special point where $T_{\mathrm{eff}} = (\sqrt{T_L} - \sqrt{T_R})^2$, both models yield identical results, as can be seen from Eq. (4). As T_R decreases further, $T_{\mathrm{eff}} > (\sqrt{T_L} - \sqrt{T_R})^2$ and the heat flux from the MCMC Maxwell bath becomes smaller than that of the standard Maxwell bath.
[46] H. P. Breuer and F. Petruccione, *The Theory of Open Quantum Systems* (Oxford University Press, Great Clarendon Street, Oxford, 2002).
[47] S. Lepri, R. Livi, and A. Politi, Phys. Rep. **377**, 1 (2003).
[48] A. Dhar, Adv. Phys. **57**, 457 (2008).
[49] G. Benenti, D. Donadio, S. Lepri, and R. Livi, Riv. Nuovo Cimento Soc. Ital. Fis. **46**, 105 (2023).
[50] M. Perarnau-Llobet, H. Wilming, A. Riera, R. Gallego, and J. Eisert, Phys. Rev. Lett. **120**, 120602 (2018).
[51] A. Rivas, Phys. Rev. Lett. **124**, 160601 (2020).
[52] P. Talkner and P. Hänggi, Rev. Mod. Phys. **92**, 041002 (2020).
[53] Á. Rivas, S. F. Huelga, and M. B. Plenio, Rep. Prog. Phys. **77**, 094001 (2014).
[54] H.-P. Breuer, E.-M. Laine, J. Piilo, and B. Vacchini, Rev. Mod. Phys. **88**, 021002 (2016).
[55] I. de Vega and D. Alonso, Rev. Mod. Phys. **89**, 015001 (2017).
[56] L. Li, M. J. W. Hall, and H. M. Wiseman, Phys. Rep. **759**, 1 (2018).
[57] D. Tamascelli, A. Smirne, S. F. Huelga, and M. B. Plenio, Phys. Rev. Lett. **120**, 030402 (2018).
[58] M. Carrega, L. M. Cangemi, G. De Filippis, V. Cataudella, G. Benenti, and M. Sassetti, PRX Quantum **3**, 010323 (2022).
[59] A. Chin, J. Keeling, D. Segal, and H. Wang, J. Chem. Phys. **163**, 050401 (2025).
[60] G. Benenti, G. Casati, K. Saito, and R. Whitney, Phys. Rep. **694**, 1 (2017).

End Matter

Appendix A: Results for two interacting particles—We generalize our Letter to the case of two interacting particles with unequal masses, a model widely used in the study of classical heat transport. The Hamiltonian of the system is given by

$$H_2 = \frac{p_1^2}{2m_1} + \frac{p_2^2}{2m_2} + g\delta(x_1 - x_2). \tag{A1}$$

Here, $g = \infty$, implying that the two particles cannot cross each other. Without loss of generality, we assume that particle m_1 is initially located on the left and particle m_2 on the right.

For the classical case, the results obtained from the MCMC simulation with Maxwell baths are shown in Fig. 5(a). It is evident that the system still exhibits the NDTR effect, consistent with the single-classical-particle scenario.

For the quantum case, the Hamiltonian (A1) can be diagonalized following the procedure described in the SM [43]. We then model the system-bath interaction operators as

$$P_L \propto \int_0^{\delta} dx_1 \int_{x_1}^{L} dx_2 |x_1, x_2\rangle\langle x_1, x_2| \tag{A2}$$

and

$$P_R \propto \int_{L-\delta}^{L} dx_2 \int_0^{x_2} dx_1 |x_1, x_2\rangle\langle x_1, x_2|. \tag{A3}$$

The quantum dynamics of the system can then be described by a Lindblad master equation, analogous to Eq. (5). The corresponding numerical results are presented in Fig. 5(b). Since we are dealing with a two-particle problem, we are limited to truncating the Hilbert space to lower energies than for a single particle. Consequently, the data in Fig. 5 are restricted to lower temperatures than those considered in the main text. Note that, denoting by N the number of particles, in the two-particle case the particle density is doubled. We therefore compare the results $J/N = J/2$ with the single-particle case, for which $J/N = J$. In contrast to the classical case, the quantum system does not exhibit the NDTR effect, in agreement with the single-quantum-particle scenario. We also observe that the heat flux is slightly reduced in the two-particle case, as expected, since the additional particle has mass $m_2 > m_1$.

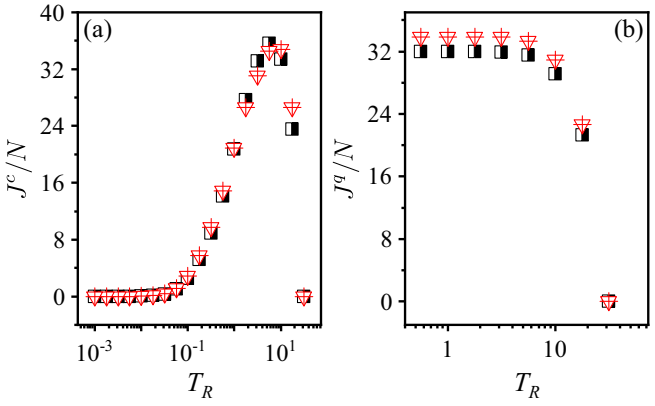

FIG. 5. Comparison of results between the two-particle (black symbols) and one-particle (red symbols) models for (a) classical and (b) quantum cases. Here, $m_1 = 1$, $m_2 = \sqrt{2}$, $T_L = 10^{1.5}$, $\eta = -2.25$, and $\gamma = 4.855$ ($\gamma = 2.891$) for the single (two) particle model is fixed by imposing the condition $\kappa^q(T_L) = \kappa^c(T_L)$.

Appendix B: Comparison of results from the Lindblad and Redfield equations—Our results in the main text are obtained using the Lindblad master equation, which relies on the secular approximation. To assess the robustness of these results, we compare them with those obtained from the Redfield equation, which does not employ this approximation and takes the form

$$\begin{aligned}\dot{\rho}(t) = -i[H_S, \rho(t)] + \sum_{\omega,\omega'} \frac{1}{2}\Gamma(\omega)\Big[&(A(\omega)\rho_S A^\dagger(\omega') \\ &- A^\dagger(\omega')A(\omega)\rho_S) + (A(\omega')\rho_S A^\dagger(\omega) \\ &- \rho_S A^\dagger(\omega)A(\omega'))\Big].\end{aligned} \tag{B1}$$

Here, $\Gamma(\omega) = J(\omega)[n(\omega) + 1]$ for $\omega > 0$ and $\Gamma(\omega) = J(|\omega|)n(|\omega|)$ for $\omega < 0$. Since the Redfield equation is not completely positive, its solutions may become unphysical in certain regimes, as the Redfield superoperator can exhibit eigenvalues with positive real parts. Therefore, we restrict our comparison to parameter regimes in which the Redfield dynamics remain physical. An illustrative comparison is provided in Fig. 6, demonstrating that the Redfield equation reproduces the Lindblad results with excellent accuracy.

Appendix C: Interaction strength between system and cold bath—In the classical MCMC Maxwell bath, the NDTR effect arises because the system-bath interaction strength effectively vanishes as the temperature approaches zero. In contrast, in the quantum case, the interaction strength does not vanish in this limit due to the wavelike nature of the quantum particle coupled to the bath.

To verify this insight, we compute the expectation value of the operator $\hat{P}_R$, which measures bath-induced transitions between energy eigenstates,

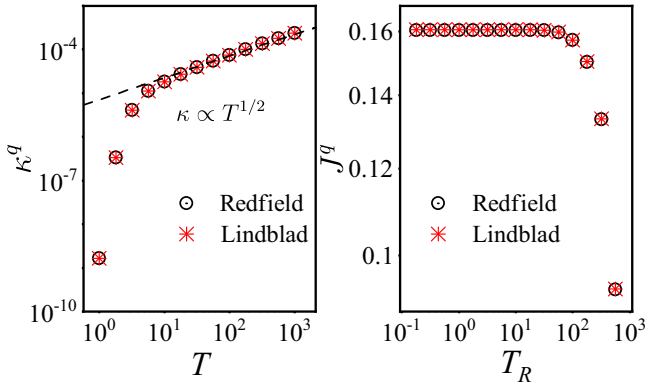

FIG. 6. Comparison between the Lindblad and Redfield equations for the heat conductivity κ^q (left) and the heat current J^q (right). Here, $\gamma = 10^{-4}$ and Hilbert space cutoff $N_{\text{tru}} = 100$. Other parameters are the same as Fig. 4 in the main text.

$$\langle \hat{P}_R \rangle = \text{Tr}(\hat{P}_R \rho_{\text{ss}}), \tag{C1}$$

where ρ_{ss} is the steady state. As shown in Fig. 7, this quantity saturates at low temperatures, in correspondence with the saturation of the quantum thermal flux. Note that, for a given interaction width δ close to the boundary, the probability of finding the quantum particle in the region $[L-\delta, L]$ scales as $1/L^3$ with the system size, leading to $\langle \hat{P}_R \rangle \propto (1/L^3)$, consistent with the vanishing of the current as one approaches the classical limit $L \to \infty$. To see the delocalization of the steady state, we compute the participation ratio in the position basis,

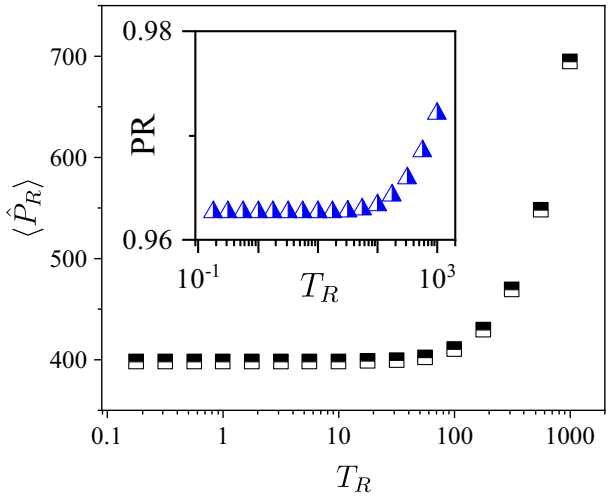

FIG. 7. Temperature dependence of average interaction strength with the cold bath. Parameters are the same as in Fig. 4 of the main text. Inset shows the cold temperature dependence of the participation ratio in the position basis.

$$\text{PR} = \frac{1}{\int_0^L dx [\rho_{\text{ss}}(x,x)]^2}. \tag{C2}$$

As shown in the inset of Fig. 7, this quantity also saturates to a finite value at low temperatures. Note that this value is close to the maximum one, namely, $\text{PR} = L = 1$ for completely delocalized (uniform) steady-state distribution.